Performance upgrades in the EUV Engineering Test Stand

Daniel A. Tichenor[*a], William C. Replogle[a], Sang H. Lee[e], William P. Ballard[a],
A. H. Leung[a], Glenn D. Kubiak[a], Leonard E. Klebanoff[a], Samuel Graham[a],
John E. M. Goldsmith[a], Karen L. Jefferson[a], John B. Wronosky[b], Tony G. Smith[b],
Terry A. Johnson[a], Harry Shields[f], Layton C. Hale[c], Henry N. Chapman[c], John S. Taylor[c],
Donald W. Sweeney[c], James A. Folta[c], Gary E. Sommargren[c], Kenneth A. Goldberg[d],
Patrick Naulleau[d], David T. Attwood[d], and Eric M. Gullikson[d]

[a]Sandia National Laboratories, PO Box 969, Livermore CA 94551
[b]Sandia National Laboratories, PO Box 5800, Albuquerque NM 87185
[c]Lawrence Livermore National Laboratory, PO Box 808, Livermore, CA 94550
[d]Lawrence Berkeley National Laboratory, One Cyclotron Road, Berkeley, CA 94720
[e]Intel Corporation, 2200 Mission College Boulevard, Santa Clara CA 95052
[f]TRW Space and Electronics Group, Redondo Beach CA 90278

ABSTRACT

The EUV Engineering Test Stand (ETS) has demonstrated the printing of 100-nm-resolution scanned images. This milestone was first achieved while the ETS operated in an initial configuration using a low power (40 watt) laser and a developmental projection system, PO Box 1. The drive laser has been upgraded to a single chain of the three-chain Nd:YAG laser developed by TRW. The resulting exposure time is ~4 seconds for static exposures. One hundred nanometer dense features have been printed in step-and-scan operation with the same image quality obtained in static printing. These experiments are the first steps toward achieving operation using all three laser chains for a total drive laser power of 1500 watts. In a second major upgrade the developmental wafer stage platen, used to demonstrate initial full-field imaging, has been replaced with the final low-expansion platen made of Zerodur[TM]. Additional improvements in the hardware and control software have demonstrated combined x and y jitter from 2 to 4 nm RMS over most of the wafer stage travel range, while scanning at the design scan speed of 10 mm/s at the wafer. This value, less than half of the originally specified jitter, provides sufficient stability to support printing of 70 nm features as planned, when the upgraded projection system is installed. The third major upgrade will replace PO Box 1 with an improved projection system, PO Box 2, having lower figure error and lower flare. In addition to these upgrades, dose sensors at the reticle and wafer planes and an EUV-sensitive aerial image monitor have been integrated into the ETS. This paper reports on ETS system upgrades and the impact on system performance.

Keywords: EUVL, lithography, optical fabrication, optical design, laser-produced plasma, laser plasma source, maglev, magnetic levitation, stages, precision engineering

1. INTRODUCTION

The EUV Engineering Test Stand (ETS) has proven to be a useful tool in acquiring the learning needed to develop commercial EUVL tools. Early last year the ETS began operation in an initial configuration which utilized a developmental projection system, low power source, developmental wafer stage platen, and a fixed reticle.[1] In this configuration 100 nm imaging in both static and scanned mode was demonstrated.[2] The ETS continues to provide data on the vacuum environment, EUV sensor development, thermal management in the illuminator, in-vacuum stage performance and EUV flare, as the major subsystems are upgraded to achieve the ETS design performance.

Upgrades are progressing in the source, projection optics and stage subsystems. The source has been re-configured to use a xenon spray-jet target, rather than the cluster-jet target used initially, and the drive laser has been upgraded from a 40 watt drive laser to the three-chain 1500 watt laser developed by TRW. Initial imaging results using a single chain are presented here. The stage system has been upgraded to incorporate

---

*Correspondence: Email: datiche@sandia.gov; telephone: 925 294 2137; Fax: 925 294 3870

a low-expansion wafer stage platen made of Zerodur™, and further modifications are in progress to enable an electrostatic reticle chuck and a reticle changer to replace fixed reticle currently installed in the ETS. The stage upgrade is discussed in section 6. The final major upgrade will replace the developmental projection system, PO Box 1, with the improved PO Box 2, having an RMS wavefront error of λ/20. Testing of PO Box 2 at the Advanced Light Source has demonstrated small-field imaging of 70 nm dense features and smaller as discussed in section 5.2.

2. ETS DESIGN OVERVIEW

The intent of the ETS design is to provide an alpha-class capability with extensive data gathering functionality to support early EUVL system learning. See Fig. 1. To proved flexible control of the vacuum environment and to enhance environmental learning, the illuminator is housed in an enclosure separate from the stages and projection system. In the illuminator the EUV radiation is generated using a laser produced plasma having a target comprised of a dense spray of liquid or frozen xenon particles. A pulsed Nd:YAG laser is focused through a window onto the xenon jet target. EUV radiation from the source is collected using a six-channel condenser, and shaped to properly illuminate the arc-shaped field of view of the projection system. A spectral-purity filter isolates the illuminator environment from the projection system environment and removes out-of-band radiation from the illuminating beam before it is incident on the reticle.
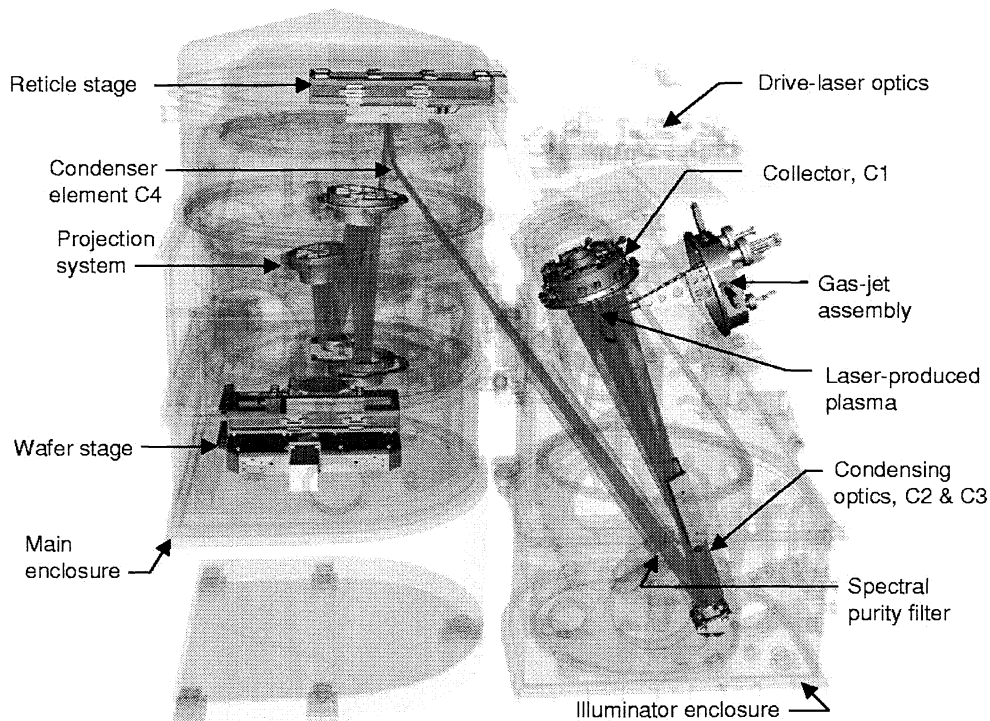
Figure 1. Solid model of the EUV Engineering Test Stand.

In the main enclosure the final condensing element, C4, shapes the illumination to cover the arc-shaped field of view. A reflecting 6 inch square reticle is carried on a magnetically levitated stage, that provides long travel in the scan direction and short travel in the remaining 5 degrees of freedom. The reticle pattern is projected onto the wafer using a 4-mirror optical system having a numerical aperture of 0.1 and producing a 4x reduction image. The wafer stage is a 1-D long travel magnetically levitated stage, similar to the reticle stage, but combined with a mechanical stage for long travel in the cross-scan direction as required to cover sites on an eight-inch wafer.

These two major modules are supported by a number of subsystems. The environment is maintained in the two modules by a vacuum system that re-circulates the xenon gas in the illuminator enclosure and regulates the gas blend in both enclosures to minimize optics contamination. Sensors are distributed throughout the system to measure pressure, temperature, gas species, EUV flux, aerial image characteristics, and pupil fill profile. A through-the-lens imager enables the user to view visible images of the reticle and wafer for tool setup functions. Finally, a control system provides flexible control for performing lithographic and environmental experiments, while collecting the sensor data and archiving it for later analysis.

3. SOURCE UPGRADE

The source upgrade involves of two major changes, the replacement of the 40 watt Coherent Infinity laser with the 1500 watt TRW laser and the replacement of the xenon cluster jet with the xenon spray jet target. The 40 watt laser enabled the initial characterization of the ETS to progress without significant thermal loading in the illuminator. A major increase in drive laser power is progressing in stages using first one chain of the TRW laser and then progressing to all three chains. While both drive sources are Nd: YAG lasers, they differ in repetition rate and pulse characteristics. The Infinity laser operates at maximum rate of 100 Hz, producing a 400 mJ pulse having a length of 4 ns. Each chain of the TRW laser operates at 1667 Hz and produces a 300 mJ pulse having a length of 10 ns. The three chains may be operated in synchronous mode, increasing the energy delivered per pulse to 900 mJ, or in interlace mode, increasing the repetition rate to 5 kHz.

For initial qualification of the ETS, the cluster jet source[3] was used at low power and with a laser-nozzle separation of 1.5 mm. This source target was found to deliver low EUV conversion efficiency, when irradiated with ~10 ns laser pulse duration which was exacerbated by nozzle heating at high average laser power. To improve conversion efficiency TRW developed the spray jet target using a 50 μm diameter orifice[4]. Operating at a stand off distance of 2 mm, stable operation was demonstrated. In this design the spray is directed forward by using a collimator located in front of the orifice. The collimator also serves as a heat shield thereby improving thermal control.

A spray jet target system, compatible with ETS space constraints, was designed, built and installed in the ETS[5,6]. See Fig 2. Xenon gas at a pressure of 2-4 MPa is liquefied using a liquid nitrogen heat exchanged located immediately upstream of the 50 μm diameter orifice. A 50 watt heater and a thermistor are embedded in the heat exchanger to control the temperature of the liquid xenon to an accuracy of ±1%.
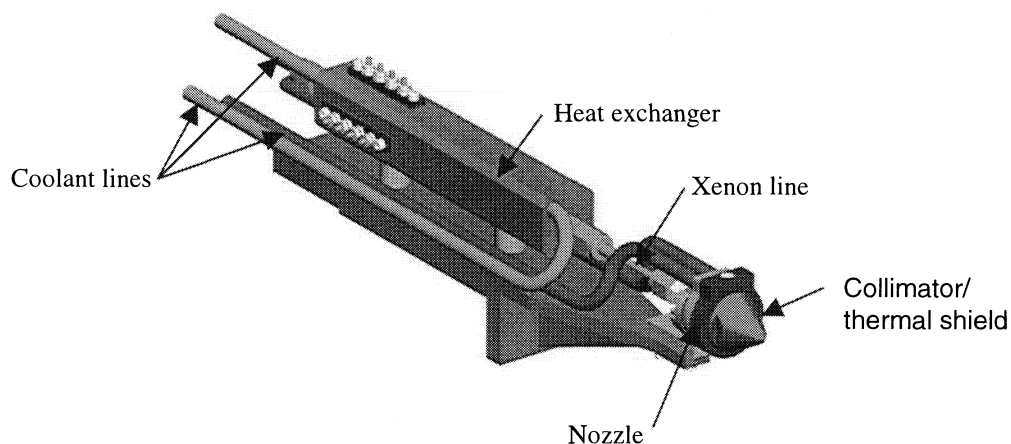
Figure 2. TRW liquid spray jet engineered for ETS compatibility.

The stability of the source output and conversion efficiency for this operating condition is shown in Fig. 3. The observed stability was sufficient for initial lithographic testing at increased drive laser power.
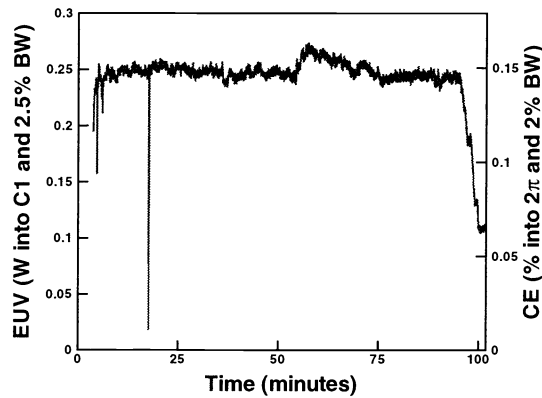
Figure 3. Ten-million-pulse source-stability test using one 500 W laser chain drive. The drive laser beam was shuttered at 20 minutes to observe the start-up transient.

4. ILLUMINATOR ENVIRONMENT

During the past year environmental data has been collected on a number of topics including cleanliness of the residual vacuum environment, as well as EUV-induced optics contamination. Residual gas analysis (RGA) data show that the ETS Main Chamber and Illuminator continue to be clean vacuum systems with high mass (> 44 amu) hydrocarbons well below 1×10^{-10} torr as reported previously[7].

The first set of C3 optics were removed from the ETS Illuminator after ~50 million laser pulses (20 months) of low power operation, and extensively characterized using Auger spectroscopy and EUV reflectance measurements[8]. EUV reflectivity data indicate a decrease in reflectivity from an initial 66% to 48-56% depending on location with more intensely illuminated areas of the C3 having a smaller final reflectivity. Measurements of the reflectivity centroid wavelength show no significant change, suggesting the observed variations were due to surface contamination and not bulk multilayer radiation damage. Auger electron spectroscopy indicates the observed reflectivity decrease can be largely attributed to carbon contamination, ~200 – 300 angstroms thick depending on location. No evidence was found for optic oxidation, indicating EtOH successfully prevented EUV/H_2O oxidation of the outermost Si layer during exposure to both EUV and out-of-band radiation. The carbon contamination was removed by RF-O_2 cleaning (See Fig. 4). Data on the effects of plasma spectrum on the plasma-facing C1 condenser optic could not be collected, since the C1 element was not available for post exposure characterization. Using high power operation the collection of C1-plasma contamination data through exposures of witness plates has been initiated.
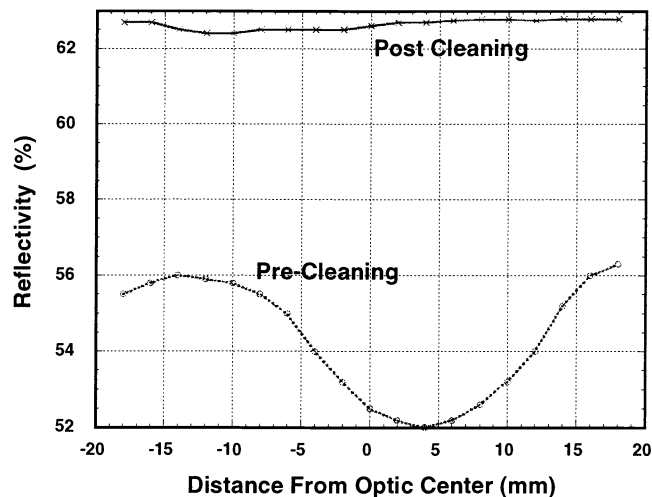
Figure 4. Reflectivity of the C3 optic before and after cleaning.

5. PROJECTION SYSTEM UPGRADE

The developmental set of projection optics (Optics Set 1) that is currently installed in the ETS will be replaced later this year. The Set 2 optic, which is of the same optical design as Set 1, is of a higher optical quality and will enable the ETS to operate as an EUV lithographic user facility. Except for high-frequency roughness (spatial periods smaller than 1 micron), almost a factor of two improvement in the figure and surface finish of the Set 2 optical surfaces was achieved as compared with the Set 1 optic[1]. The improvement in optics quality results in an optical system with lower wavefront aberration and much reduced flare, both of which lead to improved lithographic performance.

5.1 PO Box 2 fabrication and alignment

Prior to assembly into the projection optics box (POB) the mirrors were multilayer coated[9]. The change in figure error due to multilayer coating thickness variation was measured to be 0.04 nm RMS for mirror M2 and better than this for the other mirrors. This figure change should have a negligible effect on the system wavefront error. There are, however, variations of as much as 2.5% in reflectance across the mirrors, caused by variation of high spatial frequency roughness across the surfaces. It has been determined that the main effect of this is a linear variation of transmission across the image field, which can easily be compensated in the ETS[9].

The Set 2 optic was assembled in the same manner as for Set 1[1,10]. That is, the measured figure errors of the coated optics were used to recompensate the design to minimize wavefront error and distortion across the field. The mirrors were assembled to the new design with the aid of a coordinate measuring machine (CMM). The estimated accuracy of this initial assembly is better than 10 μm and 10 μrad in all degrees of freedom. The system was then aligned utilizing a visible-light interferometer[1,11]. A multi-conjugate alignment method was used to minimize wavefront and distortion measured at many points throughout the ring field, by adjusting only a small subset (eight) of the possible 24 rigid-body degrees of freedom[12]. A map of the wavefront error, measured near the center of the field, is shown in Fig. 5 and compared with the lowest wavefront error for the Set 1 optic. The wavefront error maps include spatial periods up to 108 cycles per pupil diameter, and it is seen that the RMS wavefront error has improved from 2.02 nm for Set 1 to 1.20 nm for Set 2.
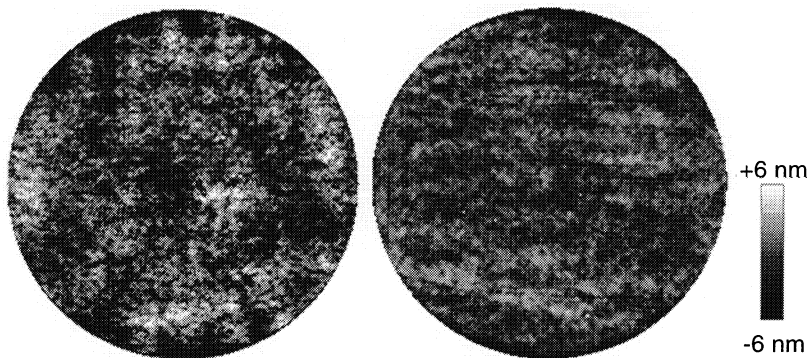
Figure 5: Wave front maps at the best field points of the Set 1 optic (left) and the Set 2 optic (right). The RMS wave front errors are 2.02 nm and 1.20 nm, respectively for the Set 1 and Set 2 optics. The maps include spatial frequencies up to 108 cycles per pupil diameter. The high-spatial-frequency detail is due to the figure of the individual mirrors and is not an artifact of the measurement.

Final optical alignment of PO Box 2 revealed an unexpected linear increase in astigmatism across the field that could not be corrected with the optical-mount actuators alone. Analysis indicates that the astigmatism can be corrected but this will require returning to the mechanical alignment step. To maintain schedule, this correction was postponed until after the ALS static imaging experiments described in Section 5.2. The

alignment will be corrected prior to inserting PO Box 2 into the ETS. When the alignment is corrected, the cause of this unexpected result will be determined.

5.2 PO Box 2 characterization using EUV radiation

To acquire early learning in high resolution EUV imaging in parallel with ongoing system integration of the ETS using PO Box 1, the Sub-field Exposure Station (SES) was developed at the Advanced Light Source. The SES was realized by modifying the phase-shifting point-diffraction interferometer facility[13] used to measure the wavefront error in PO Box 1 and PO Box 2 (See Figure 6). The major change required for printing was the design and installation of a new illuminator to provide partially coherent illumination rather than coherent illumination required for interferometry. This illuminator incorporates an actuated mirror that scans a small spot in the projection system aperture to generate an arbitrary pupil fill pattern during the exposure. The resulting illuminator can generate a conventional "top hat" fill having partial coherence (σ) ranging from 0.2 to 1. Other pupil fill profiles have also been demonstrate in the SES, including annular, dipole and the ETS 6 channel fill. The illuminated sub-field is 100 μm in diameter at the wafer plane, and the illumination can be moved to characterize the entire well-corrected field, one sub-field per exposure.
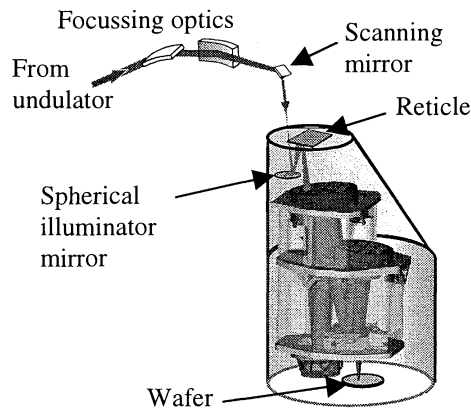
Figure 6. Sub-field Exposure Station at the Advanced Light Source. This system was developed to acquire early images using PO Box 2 in parallel with ETS system integration using PO Box 1.

PO Box 2 was installed in the SES, and test patterns of sub-100 nm features have been printed using various pupil fill profiles[14]. Examples of 70 nm and 80 nm dense elbows are shown in Figs. 7 and 8. As expected, the resolution is significantly improved compared to the 100 nm dense features printed using PO Box 1 in the ETS[1]. The image quality at 70 nm is at least as high as that of 100 nm features printed using PO Box 1. In particular, the iso-dense bias is less apparent in the PO Box 2 images (70 nm) than in the PO Box 1 images (100 nm) printed in the ETS as shown in section 8.

80 nm elbows   70 nm elbows
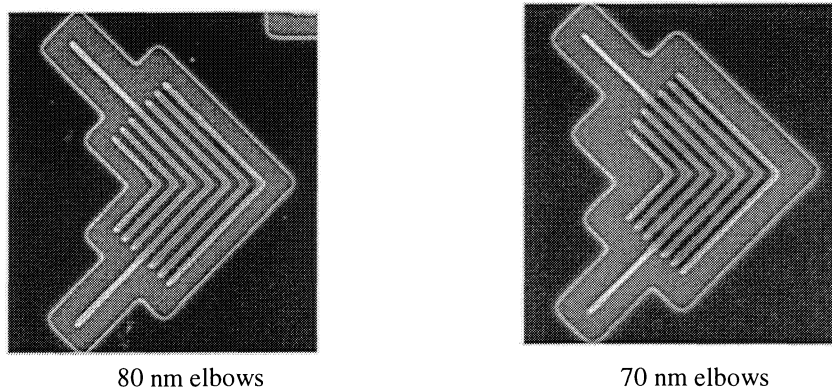
Figure 7. PO Box 2 images acquired in the SES using the ETS 6-channel pupil fill.
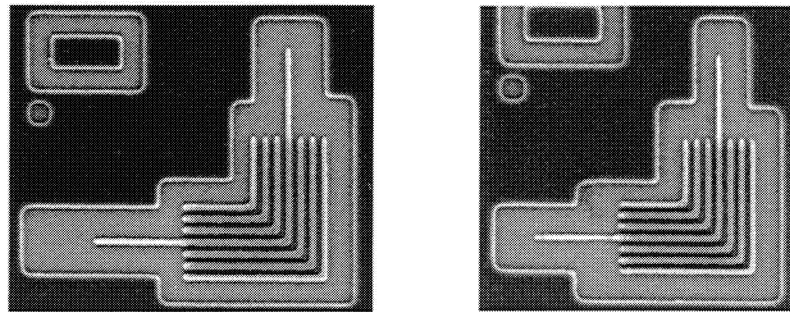
80 nm elbows   70 nm elbows

Figure 8. PO Box 2 images acquired in the SES using a top-hat pupil fill with $\sigma = 0.7$.

In addition to interferometry and sub-field imaging, the flare of the Set 2 optic has been measured across the field of view using a knife-edge test. The observed flare is constant to within the measurement error[15,16]. This result implies that CD variation, caused by variation of flare across the field, will be small. In addition, it was found that the flare of the Set 2 optic is less than half that of the Set 1 optic. The flare in a dark 1-micron wide line in a bright field is 40% for the Set 1 optic and 17% for the Set 2. The integration of PO Box 2 in the ETS, with the demonstrated reduction in wavefront error and flare, is expected to achieve the performance goal of printing 70 nm dense features in full-field scanned imaging.

6. STAGE SYSTEM

The magnetically levitated stage system has been operating in the ETS for the past year. Both the wafer stage and reticle stage have performed to specifications needed for initial lithography experiments using a low power source. Evolving performance requirements, high-power source integration, and desired stage system reliability improvements have provided a path for recent stage system upgrades. Figures 9 and 10 show the reticle and wafer stages outside the ETS.
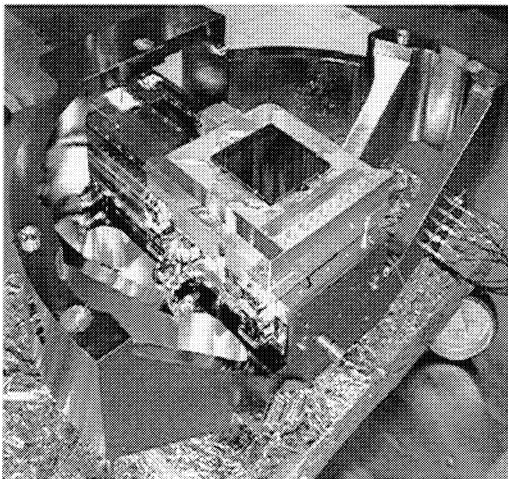
Figure 9. Reticle stage inverted with support structure.
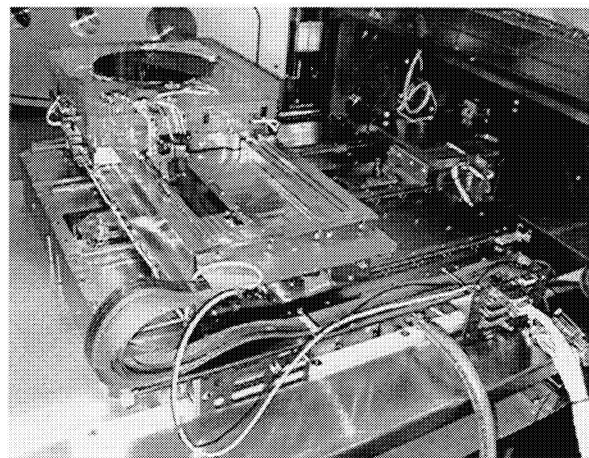
Figure 10. Wafer stage on handling cart.

The wafer and reticle stage subsystem consists of maglev reticle and wafer stages, metrology for each stage, and control electronics. A feedback control system provides synchronization of the reticle and wafer stages during exposures. The wafer stage must track the reticle stage during scanning of the reticle stage through the EUV field. Throughput, structural stability, critical dimension, and wafer exposure characteristics determine stage subsystem limits for acceleration, scan speed, settle time, and dynamic stability. The ETS

requires each stage as referenced to the PO box to operate with less than 7 nm (RMS) of X and Y jitter. The Z (focus) error must be less than 75 nm (mean+3 sigma). These specifications must be maintained while scanning the wafer at 10 mm/s. Performance to these specifications has been demonstrated in the ETS.

6.1 Stage subsystem progress during 2001

Lithography results reported in 2001[1,17] included static imaging and slow scanning (~ 10 μm/s at the wafer) for 100 nm features. At that time, the stages met these requirements over a limited travel range. The effort over the last year has included mechanical improvements and performance development to meet full ETS performance requirements. The improvements have facilitated performance consistent with 70 nm feature imaging using the ETS high power source. The continuing development is aimed at providing the reliability needed for the ETS User Facility in 2002.

6.2 Stage hardware improvements

Changes to the stages include integration of the Zerodur wafer stage platen with an improved assembly configuration, improved cable routing, new cable design, and improved metrology surface flatness.

The Zerodur platen assembly was changed to eliminate the use of threaded inserts that created an overstress condition in the platen. The modification replaces the inserts with much larger pads to spread out the forces and not preload the platen. With the elimination of the preloaded screw connections, the limiting design loads become the externally applied forces on the structures. Finite element analysis shows that the maximum stress in the Zerodur has been reduced by an order of magnitude. In order to minimize deformation of the metrology mirror surfaces on the platen caused by a temperature gradient in the linear motor magnet array, and maintain high platen assembly structural resonance, a new flexure design was implemented in the magnet array. The Zerodur platen assembly is shown in Fig. 11. An aluminum platen with a well characterized mirror surface is being used for the reticle stage. The Zerodur platen is needed at the wafer to manage thermal expansion caused by actuator and sensor thermal loads.
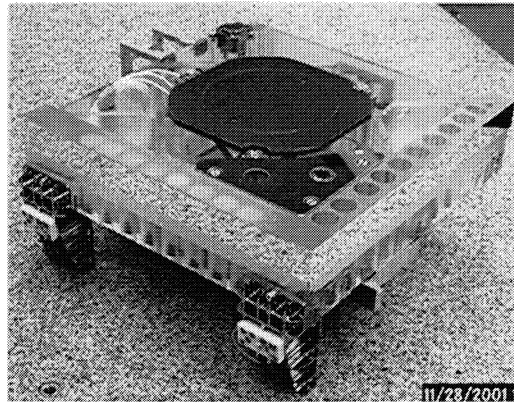
Figure 11. Wafer stage platen assembly.

Improvements to moving cables and their routing and attachment have been completed to address infrequent non-repeatable position disturbances and to accommodate previous changes to both stages. This included replacement of an integrated cable/capacitive sensor and redesign of all moving cables and attachment brackets to optimize cable roll during scanning.

6.3 Performance development

A systematic approach to performance development has resulted in stage performance that facilitates 70 nm feature imaging. Scanning speeds of 10 mm/s (40 mm/s at the reticle stage) are now routine. The approach includes: error source identification, control optimization, repeatable error mapping, and minimization of non-repeatable errors.

Significant performance improvement has resulted from the application of feed-forward techniques to minimize repeatable errors. Several applications have been implemented and others are under consideration. Maps of the platen mirrors are produced using high-resolution interferograms combined with data taken

during stage scanning. Maps are then used during stage operation to correct for mirror non-flatness. These maps where then verified through wafer printing and analysis. Currently, mirror mapping is being used only on the reticle stage, as the new Zerodur wafer stage platen has not required additional correction.

The force variability of the bearings[17] used in the maglev stages employed in the ETS stage system provide several opportunities for performance improvement using feed-forward techniques. Stage static position performance has been improved by using the gap-related force profile produced by the gravity-offsetting permanent magnets and using the information during stage control. Additionally, repeatable forces appear as the stage is scanned. Feed-forward techniques have been applied to the stage controller to compensate for these position and velocity related disturbances.

Other repeatable errors have been found related to the interactions between control method and metrology. While these are often the most difficult to identify, they have been reduced as part of the development process. Work continues toward performance optimization over the full travel range of the wafer. Several additional techniques will be investigated over the next year.

6.4 Stage system performance

While some position dependent performance issues remain, performance across the wafer is typically well within specifications. Figure 12 shows wafer stage jitter and focus performance seen while scanning a wafer die site.
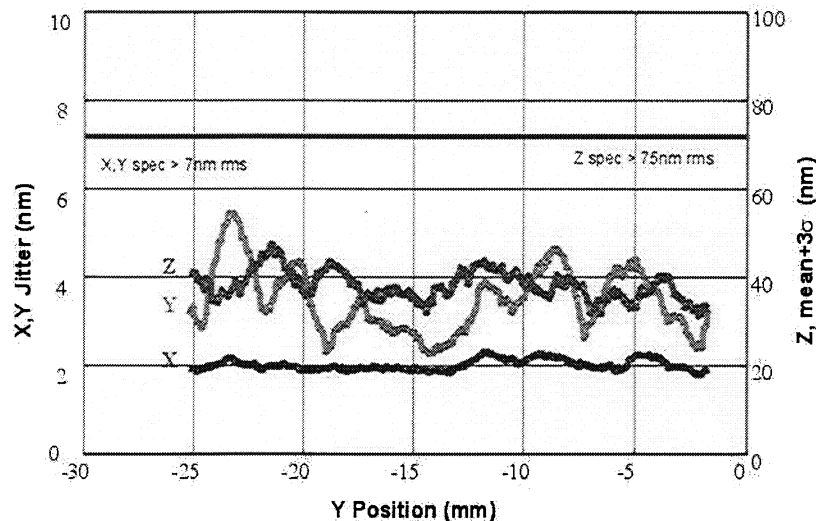
Figure 12. Wafer stage performance scanning at 10 mm/s.

A procedure for calculating stage parameters that are important to the imaging performance of the ETS has been developed to track stage performance as ongoing improvements are made. The procedure examines the two basic categories of errors: image jitter and focus error. Figure 13 illustrates recent results from this metric. The plot represents the combined position error from both the wafer and reticle stages for five representative die sites across the wafer.
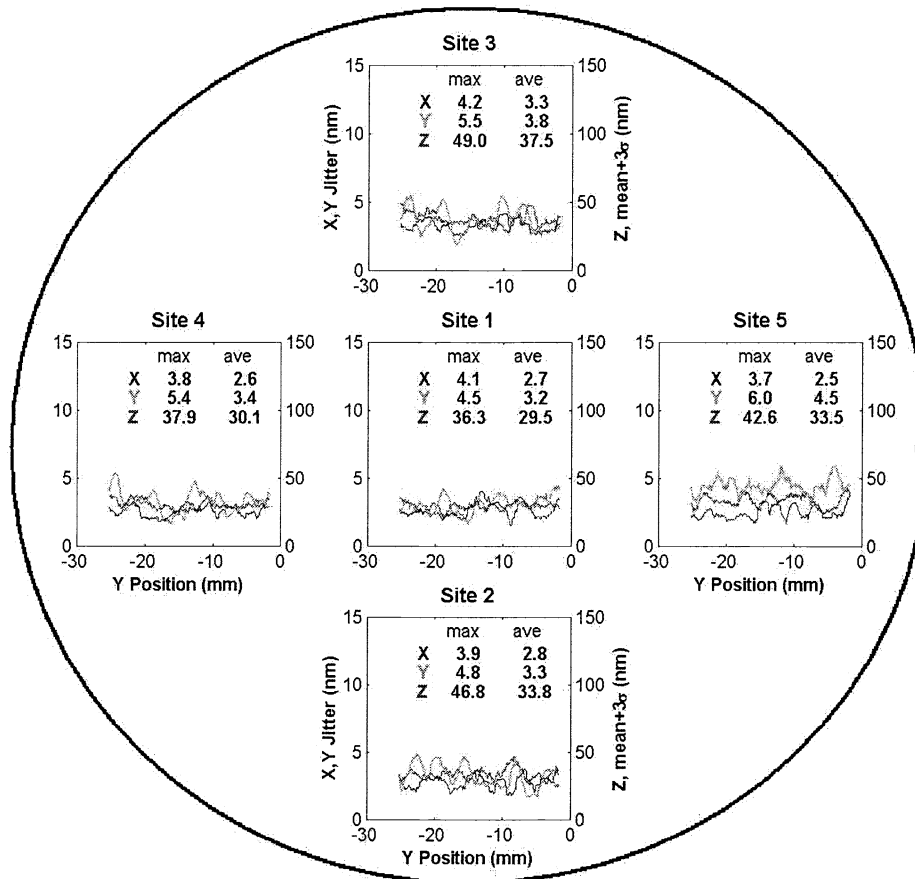
Figure 13. Jitter and focus error for five representative die sites.

7. EUV SENSORS

A variety of EUV-specific sensors have been incorporated into the ETS in addition to temperature sensors, vibration monitors, vacuum gauges, residual gas monitors, etc. These sensors include wavelength-filtered photodiodes nested within the first condenser elements to monitor source output, EUV CCD cameras that monitor the source size and position, an EUV photoemission sensor that monitors the signal from the final condenser element, dose/illumination distribution sensors at the reticle and wafer planes, and an aerial image monitor (AIM) sensor at the wafer plane. The latter three have become operational during the past year. They incorporate AXUV-HS5 photodiode elements (International Radiation Detectors, Inc.) into packages with customized electronics to provide the desired functionality. The active area of the photodiodes has been coated with a 200-nm-thick layer of zirconium to serve as a spectral filter.

7.1 Reticle stage dose/illumination distribution sensor

The primary function of the reticle-stage dose sensor is to measure the distribution of the EUV illumination at the reticle plane. Because the reticle stage has significant travel only in the scan direction, the desired functionality could not be provided by a single detector element. The sensor has therefore been implemented as a linear array of photodiode elements positioned on the reticle stage adjacent to the reticle. The illumination pattern is mapped out by using the reticle stage to scan the array across the EUV ring field.

The sensor consists of four segments, each containing 20 elements on 1.65 mm centers. The segments are butted together to create an 80-element detector array, positioned behind an array of 100 μm pinholes that precisely define the sensed regions. On-stage electronics amplify, digitize, and process the signals from the

individual elements to eliminate noise pick-up and simplify cabling to the on-stage components. The sensor and a representative illumination profile are shown in Fig. 14.
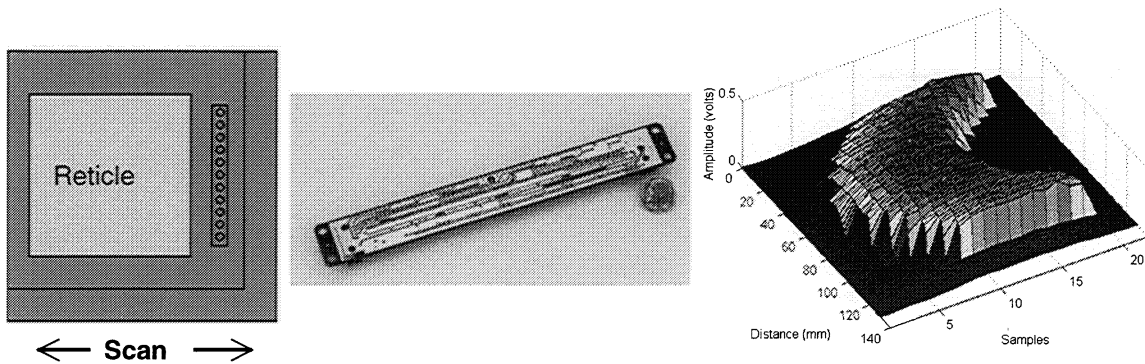
Figure 14. Implementation of reticle dose sensor (left), linear array hybrid (center), and measurement of reticle-plane illumination distribution (right).

7.2 Wafer-stage dose sensor

Because the wafer stage has a long travel range in both transverse directions, a single sensor element can be used for the dose sensor. The sensor, located in one corner of the wafer platen as shown in Fig. 15, is positioned behind a 25-μm pinhole to provide a well defined detection area, needed for absolute calibration. Similar to the reticle-stage dose sensor, on-stage electronics include an amplifier, multiplexer (to select the dose or AIM sensor), digitizer, and processing electronics. In addition to measuring the spatial distribution of EUV radiation at the wafer plane (Fig. 15), this sensor provides measurements of the absolute pulse energy at the wafer.
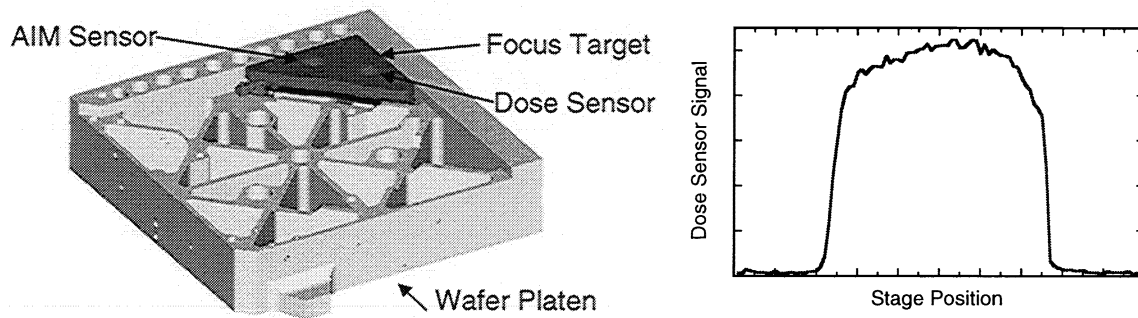
Figure15. Location of the dose and AIM sensors on the wafer platen (left). Wafer dose sensor scan across the field of view in the scanning direction (right).

7.3 AIM sensor

An Aerial Image Monitor (AIM) sensor has also been implemented on the wafer platen (Fig. 15). High spatial resolution is achieved by placing a patterned structure in front the detector assembly. The patterned structure, or AIM artifact, consists of 100-nm-wide slits, etched into a nickel absorber on an EUV-transparent, silicon nitride membrane as shown in Fig. 16. The slits are 100 μm long and replicated 10 times to increase the collection area and the resulting signal strength. In operation the AIM detector scans across a periodic pattern in the aerial image that has the same pitch (10 μm) as the AIM artifact. The photodiode assembly employs a higher-gain preamplifier, but is otherwise similar to that of the wafer dose sensor. Much of the on-stage electronics is shared between the two sensors.
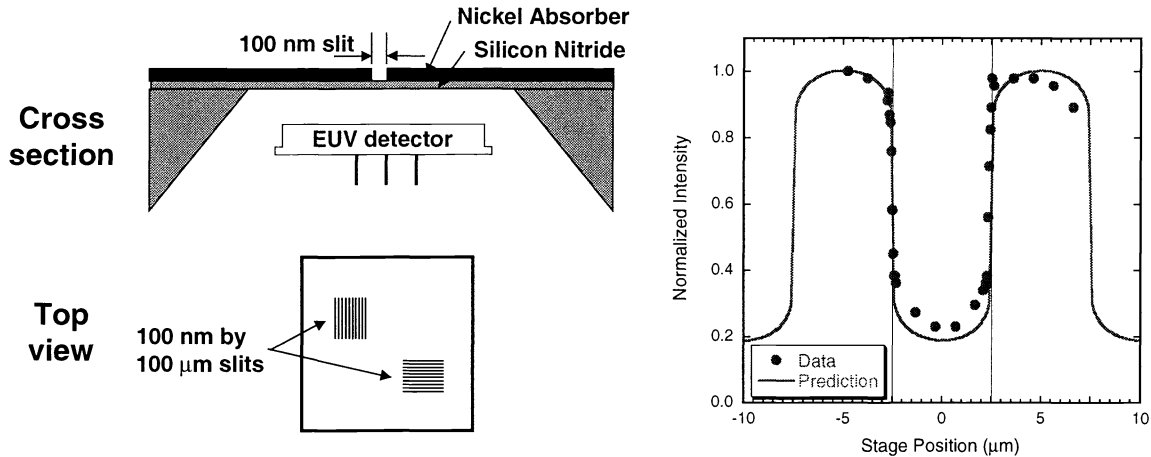
Figure 16. Schematic of Aerial Image Monitor (AIM) detector assembly (left). Data acquired by scanning the AIM detector across an array of 5 micron wide lines and spaces (right).

Fig. 16 also shows a measurement acquire by using a mask pattern consisting of 5-micron-wide 1:1 lines and spaces as imaged onto the wafer. The circles represent an average of 200 laser pulses, with the wafer stage translated in 1-micron steps on the flatter portions of the profile, and in 50-nm steps on the steep portions of the profile. The solid curve is an aerial image simulation normalized to the peak of the AIM measurement with no other adjustable parameters. The significant rounding of the corners and the nonzero signal in the dark lines are caused by the known flare present in the Set 1 optics. The AIM sensor can be used for a variety of measurements, including finding focus and monitoring focus stability, measuring drift or jitter between the EUV image and the wafer stage, determining scan magnification and skew, and studying image distortion.

8. HIGH-POWER IMAGING RESULTS

Lithographic experiments were performed to demonstrate scanned imaging using the high-power source (one laser chain) and to validate system changes including the wafer stage upgrade[18]. In these initial high-power tests a conservative source configuration was used to reduce environmental risk to the condenser. In this configuration a 50 μm orifice was used to provide a more stable and reliable source. A smaller orifice is being developed to reduce the ambient gas pressure. The plasma-to-nozzle stand off distance was set to 4 mm to minimize environmental risk to the C1 collector. Finally, the use of one laser chain (500 watts), versus all three chains, further limits throughput, but also reduces the thermal load. Ongoing source work is directed toward increasing the EUV throughput and maintaining a high degree of source stability. This source configuration provides an EUV output of 15-to-30 times greater than low power operation and an EUV stability of about 5% peak-to-peak during most of the lithographic exposures. While this is only a step toward higher EUV throughput, it is a sufficient increase to provide additional learning from lithographic experiments.

Since the stage system had been modified subsequent to the scanning experiments performed last year, it was necessary to determine the new scan skew angle. In two iterations the skew was determined to be -210 microradians, which is easily accommodated by the stage range of motion. Scan magnification difference form the 0.25 design value was measured to be +90 ppm, which is unchanged, to within the measurement accuracy, from the value determined last year. Using these parameters resist images of features down to 90 nm dense lines were printed at a wafer scan speed of 0.14 mm/s as shown in Fig.17.

90 nm 100 nm 130 nm
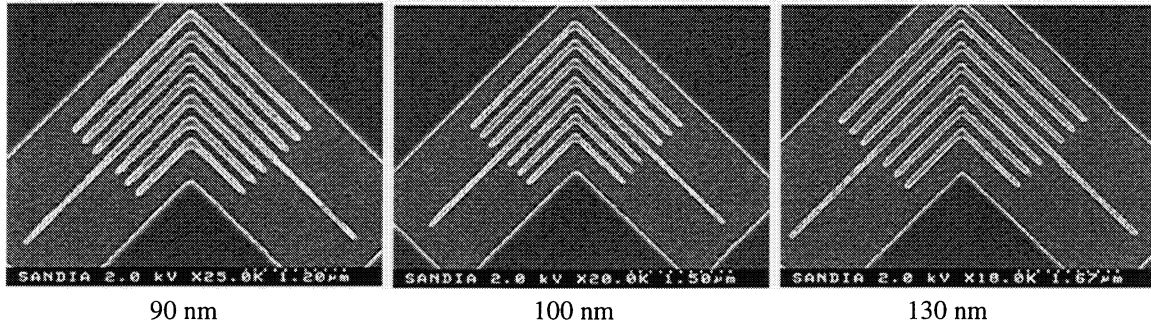
Figure 17. ETS scanned images of 45° elbows at various feature sizes.

To further evaluate ETS performance static images are compared to scanned images. As shown in Fig. 18, the quality of the scanned images of 100 nm features is indistinguishable from that of the static images. This verifies that the scan magnification and skew have been accurately determined. It further verifies that the scan distortion across the field of view is small, and that stage jitter remains small in both static and scanning operation.
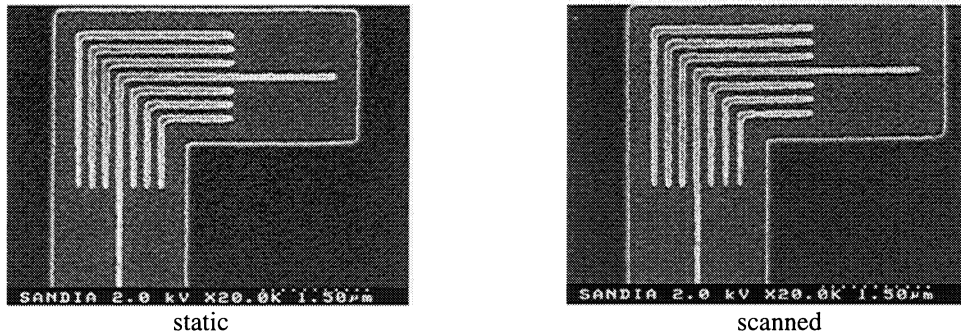
static scanned

Figure 18. ETS images of 100 nm elbows recorded in static (left) and scanned (right) mode.

9. EUVL USER FACILITY

Completion of ETS performance upgrades is planned for the coming year. The ETS will then become an important tool in the EUVL User Facility with the objective of continuing the learning required to support commercialization of EUV lithography. The ETS will be a vehicle for learning in a number of areas summarized in Table 1.

Table 1. Summary of ETS-based EUVL learning. – current and ongoing learning, > future learning.

• **Lithographic learning**	• **System learning**
– Static and scanned imaging	– Vibration environment
– Flare measurements	– Thermal management
– Resist characterization	– Vacuum system development
– Dose control	• **Source characterization**
➤ Process window measurement	– Conversion efficiency
➤ CD control	– EUV output stability
• **Environmental learning**	– Source-related environmental testing
– Condenser lifetime	➤ New source configurations
– Contamination mitigation	• **Sensor development**
➤ Projection system lifetime	– EUV dose sensors
➤ In-situ cleaning	– Aerial Image Monitor
➤ Resist outgassing	– Through-the-lens imaging
	– Pupil fill visualization
	➤ New EUV sensor testing

10. SUMMARY

Three major subsystem upgrades are progressing in the ETS. The stage system upgrade has been completed, and the measured performance is ~2 times better than the 7 nm RMS jitter specification required to support 70 nm printing. Progress on the source upgrade includes the conversion to the xenon spray jet target and the use of the TRW drive laser at an average power of 500 watts. Using this system configuration and with the developmental projection system installed, dense features down to 90 nm have been printed in step-and-scan operation. The quality of scanned images is comparable to that observed for static printing. Sub-field imaging using an improved projection system has demonstrated the printing of 70 nm dense features. Based on these results, a substantial improvement in the resolution of full-field EUV images is expected, when the ETS upgrades are completed during the coming year. The ETS is an increasingly important tool in the EUVL User Facility to advance EUV learning as required for commercialization.

ACKNOWLEDGMENTS

REFERENCES

1. D. A. Tichenor, A. K. Ray-Chaudhuri, W. C. Replogle, R. H. Stulen, G. D. Kubiak, P. D. Rockett , L. E. Klebanoff, K. L. Jefferson, A. H. Leung, J. B. Wronosky, L. C. Hale, H. N. Chapman, J. S. Taylor, J. A. Folta, C. Montcalm, R. Soufli, E. Spiller, K. Blaedel, G. E. Sommargren, D. W. Sweeney, P. Naulleau, K. A. Goldberg, E. M. Gullikson, J. Bokor, P. J. Batson, D. T. Attwood, K. H. Jackson, S. D. Hector, C. W. Gwyn, and P. Y. Yan, "System Integration and Performance of the EUV Engineering Test Stand," *Emerging Lithographic Technologies V*, Proc. of SPIE vol. 4343, 19-37 (2001).
2. D. A. Tichenor, A. K. Ray-Chaudhuri, S. H. Lee, H. N. Chapman, W. C. Replogle, K. W. Berger, R. H. Stulen, G. D. Kubiak, L. E. Klebanoff, J. B. Wronosky, D. J. O'Connell, A. H. Leung, K. L. Jefferson, W. P. Ballard, L. C. Hale, K. Blaedel, J. S. Taylor, J. A. Folta, E. Spiller, R. Soufli, G. E. Sommargren, D. W. Sweeney, P. Naulleau, K. A. Goldberg, E. M. Gullikson, J. Bokor, D. T. Attwood, U Mickan, R. Hanzen, E. Panning, P. Y. Yan, J. E. Bjorkholm, and C. W. Gwyn, "Initial results from the EUV Engineering Test Stand," *Soft X-Ray and EUV Imaging Systems II*, Proc. of SPIE vol. 4506, 9-18 (2001).
3. G.D. Kubiak, L. J. Bernardez, and K. D. Krenz, "High-power Extreme Ultraviolet Source Based on Gas Jets," in *Emerging Lithographic Technologies II*, Y Vladimirsky, Ed., Proc. SPIE, Vol. 3331, 81-89, (1998).
4. R. H. Moyer, H. Shields, A. Martos, S. W. Fornaca, R. J. St. Pierre, and M. B. Petach, "Laser-Produced Plasma (LPP) Scale-up and Commercialization," in *Emerging Lithographic Technologies V*, E. A. Dobisz, Ed., Proc. SPIE, Vol. 4343, 249-254, (2001).
5. W. P. Ballard, L. J. Bernardez, R. E. Lafon, R. J. Anderson, H. Shields, M. B. Petach, and R. J. St.Pierre, "High-Power Laser-Produced-Plasma EUV Source," These proceedings (2002).
6. H. Shields, S. W. Fornaca, M. B. Petach, M. Michaelian, R. D. McGregor, R. H. Moyer, and R. St. Pierre, "Xenon Target Performance Characteristics for Laser_Produced Plasma EUV Sources," These proceedings (2002).
7. L. E. Klebanoff, M. E. Malinowski, P. Grunow, W. M. Clift, C. Steinhaus, A. H. Leung, and S. J. Haney, "First Environmental Data from the EUV Engineering Test Stand," *Emerging Lithographic Technologies V*, Proceeding of SPIE Vol. 4343, 342-346, (2001).
8. L. E. Klebanoff, P. A. Grunow, A. H. Leung, S. J. Haney, and M. E. Malinowski, "Environment Data from the EUV Engineering Test Stand (ETS)," These proceedings (2002).

9. R. Soufli, E. Spiller, M. A. Schmidt, J. C. Davidson, R. F. Grabner, E. M. Gullikson, B. B. Kaufmann, S. Mrowka, S. L. Baker, H. N. Chapman, R. M. Hudyma, J. S. Taylor, C. C. Walton, C. Montcalm, and J. A. Folta, "Multilayer optics for an extreme-ultraviolet lithography tool with 70-nm resolution," *Emerging Lithographic Technologies V*, Proc. of SPIE vol. 4343, 51-59, (2001).

10. H. N. Chapman, A. K. Ray-Chaudhuri, D. A. Tichenor, W. C. Replogle, R. H. Stulen, G. D. Kubiak, P. D. Rockett, L. E. Klebanoff, D. O'Connell, A. H. Leung, K. L. Jefferson, J. B. Wronosky, J. S. Taylor, L. C. Hale, K. Blaedel, E. A. Spiller, G. E. Sommargren, J. A. Folta, D. W. Sweeney, E. M. Gullikson, P. Naulleau, K. A. Goldberg, J. Bokor, D. T. Attwood, U. Mickan, R. Hanzen, E. Panning, P.-Y. Yan, C. W. Gwyn, and S. H. Lee, "First lithographic results from the EUV engineering test stand," J. Vac. Sci. Technol. B **19**, 2389-2395 (2001).

11. K. A Goldberg, P. Naulleau, J. Bokor and H. N. Chapman, "Honing the accuracy of extreme ultraviolet optical system testing: at-wavelength and visible-light measurements of the ETS Set-2 projection optic," These proceedings (2002).

12. H. N. Chapman and D. W. Sweeney, "A rigorous method for compensation selection and alignment of microlithographic optical systems," Proc. SPIE Vol. 3331, 102-113 (1998).

13. P. Naulleau, K. Goldberg, E. Anderson, P. Batson, P. Denham, S. Rekawa, and J. Bokor, "Adding static printing capabilities to the EUV phase-shifting point diffraction interferometer," *Emerging Lithographic Technologies V*, Proceeding of SPIE, **4343**, 639-645, (2001).

14. P. Naulleau, K. A. Goldberg, E. H. Anderson, D. T. Attwood, Jr., P. J. Batson, J. Bokor, P. Denham, E. M. Gullikson, B. Hoef, K. H. Jackson, S. Rekawa, F. Salmassi, K. L. Blaedel, H. N. Chapman, L. C. Hale, R. Soufli, E. A. Spiller, D. W. Sweeney, J. S. Taylor, C. C. Walton, G. F. Cardinale, A. K. Ray-Chaudhuri, A. Fisher, D. J. O-Connell, R. H. Stulen, D. A. Tichenor, C. W. Gwyn, P. Yan, and G. Zhang, "Static microfield printing at the Advanced Light Source with the ETS Set-2 optic," These proceedings (2002).

15. P. Naulleau, K. A. Goldberg, E. H. Anderson, P. Batson, P. E. Denham, K. H. Jackson, E. M. Gullikson, S. Rekawa, and J. Bokor, "At-wavelength characterization of the extreme ultraviolet Engineering Test Stand Set-2 optic," J. Vac. Sci. Technol. B **19**, 2396-2400 (2001).

16. E. M. Gullikson, K. A. Goldberg, P. Naulleau, J. E. Bjorkholm, S. H. Lee, H. N. Chapman, S. L. Baker, J. S. Taylor, and D. A. Tichenor, "The Prediction and Measurement of Flare," International Sematech workshop on EUV Lithography, October 29, 2001, Matsue, Japan.

17. Tony G. Smith, John B. Wronosky, Terry A. Johnson, Pat S. Barney , Joel R. Darnold, "A Linear Magnetic Bearing Application: Scanning Stages for EUV Lithography", "*2001 Summer Topical Meeting*", ASPE proceedings of: Precision Bearings and Spindles, June 18, 19, (2001).

18. S. H. Lee, D. A. Tichenor, W. P. Ballard, L. J. Bernardez II, J. E. M. Goldsmith, S. J. Haney, K. L. Jefferson, T. A. Johnson, A. H. Leung, D. J. O'Connell, W. C. Replogle, J. E. Bjorkholm, E. Panning, P. Naulleau, K. A. Goldberg, H. N. Chapman, G. D. Kubiak, and C. W. Gwyn, "Lithographic evaluation of the EUV engineering test stand," These proceedings (2002).